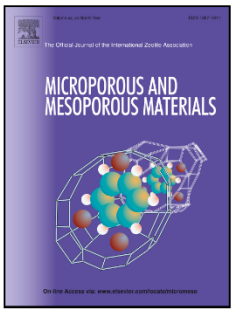

Zeolites fit for a crown: Studying organic-framework host-guest interactions through thermogravimetric techniques

Antony Nearchou, Rémi Castaing, Paul R. Raithby, Asel Sartbaeva

PII: S1387-1811(20)30481-9

DOI: https://doi.org/10.1016/j.micromeso.2020.110479

Reference: MICMAT 110479

To appear in: *Microporous and Mesoporous Materials*

Received Date: 15 October 2019

Revised Date: 11 May 2020

Accepted Date: 6 July 2020

Please cite this article as: A. Nearchou, Ré. Castaing, P.R. Raithby, A. Sartbaeva, Zeolites fit for a crown: Studying organic-framework host-guest interactions through thermogravimetric techniques, *Microporous and Mesoporous Materials* (2020), doi: https://doi.org/10.1016/j.micromeso.2020.110479.

Author Contributions

The manuscript was written by A.N. and proof read by all the co-authors. Sample preparation and analyses were per-formed by A.N. R.C. helped with the TG and DTA setup, in addition to the means of analysing and interpreting the data. Both A.S. and P.R.R. aided in the data interpretation.

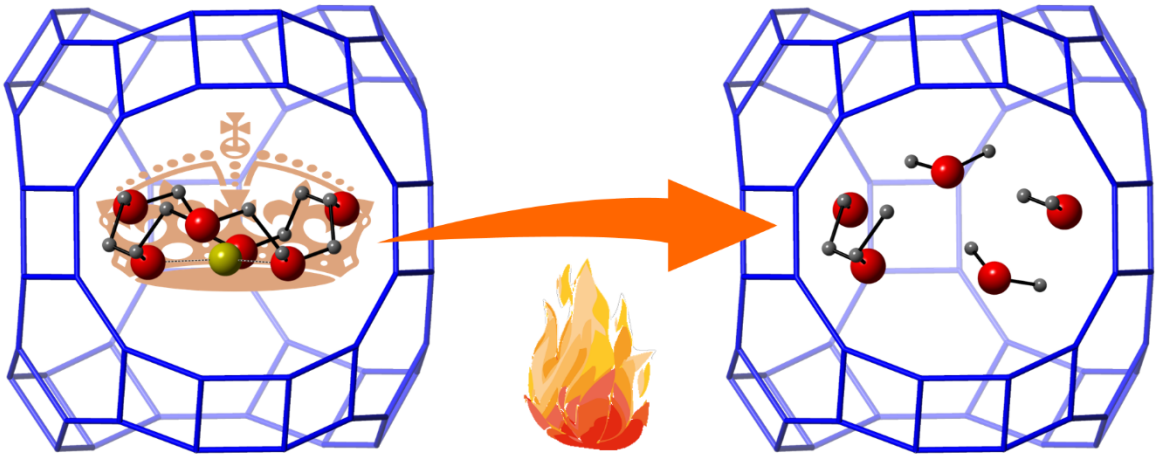

Zeolites fit for a crown: studying organic-framework host-guest interactions through thermogravimetric techniques

Antony Nearchou, [a] Rémi Castaing, [a] Paul R. Raithby [a] and Asel Sartbaeva *[a]

[a]University of Bath, Department of Chemistry, Claverton Down, Bath, BA2 7AY, UK
*A.Sartbaeva@bath.ac.uk

Abstract

Every year millions of tons of zeolites are produced, being used as molecular sieves, hydrocracking catalysts, gas-capture materials and for emerging novel applications. There is a demand to synthesise new zeolites with bespoke frameworks, which are tailor-made for a chosen application. To achieve these 'designer zeolites' it is crucial to fully understand the host-guest interactions between organic additives and zeolitic frameworks. Here we have studied four different zeolites, synthesised with the same organic additive, 18-crown-6 ether, which show observable differences in the host-guest interactions. We demonstrate that the framework geometry dominates the decomposition temperature, enthalpy and mechanism. The zeolites show unique decomposition features, emphasising experimental differences in how the organic additive and framework interact.

Introduction

Zeolites have a variety of uses across the chemical sciences, such as catalysts for organic chemistry, molecular sieving, carbon dioxide capture and many other emerging applications.[1-3] To this day, zeolites are still the primary catalyst used for petroleum hydrocracking, demonstrating their contemporary robustness that has not been replaced via alternative porous materials.[4] It is this robustness, combined with their size and shape-selectivity, that make zeolites such ideal solid state catalysts. Consequently, there is a desire in the community to prepare new designer zeolites which possess bespoke structures to enhance chosen chemical applications.[5-9] This has since been highlighted by Science, where steps towards tailor-making zeolites have been listed in the top ten breakthroughs of 2011.[10]

Current approaches towards designer zeolites make use of organic additives, which direct the crystallisation of a desired topology. The addition of organics was first reported in 1961 by Barrer et al.[11] but it was not until 1967 that the use of additives was utilised to crystallise a new zeolite; high-silica zeolite beta.[12] As it is, the use of organic additives is a necessity for the preparation of new zeolites, being needed to construct the desired structure. An organic additive's involvement in synthesis consists of non-bonding, van der Waals interactions with the assembling silica oligomers.[13-15] These organic-framework host-guest interactions are integral in discriminating which framework is grown.[16]

Organic additives can be subdivided into space-filling species, organic structure directing agents (OSDAs) and true templates, depending on the degree and nature of these interactions.[14] One of the methodologies employed to prepare new zeolites is to use computer simulations to predict which additives have the most favourable non-bonding interactions with the framework.[15, 17] However, these techniques only consider true templating and the distinct nature of these interactions in

To glean experimental information on these organic-framework host-guest interactions we have studied zeolites Na-X (FAU), EMC-2 (EMT), RHO and ZK-5 (KFI). All four zeolites express unique structures, as shown in figure 1, however they can all be prepared using 18-crown-6 ether (18C6) as an organic additive.[18- 24] Interestingly, all of the zeolites can be synthesised in the absence of 18C6,[22, 25, 26] aside from zeolite EMC-2 where 18C6 appears to be a necessity in order to influence the free-energy of crystallisation and prevent formation of FAU-type zeolites.[23, 27] The 18C6 molecule itself is known to be flexible, with the molecule's dimensions being deeply dependant on its conformation. The lowest energy conformations, as seen via calculations and experimentally, are the D_{3d} and C_i conformations which have molecular lengths of 8.6 Å and 6.9 Å, respectively.[28] Figure 1 shows the aperture sizes of the cages the 18C6 molecule is known to occupy,[21, 29-31] which when considering the 18C6 molecular length emphasises how it will experience confinement and host-guest interactions within the frameworks. Amongst the zeolites, synthetic parameters such as incubation time, hydrothermal conditions and the Si/Al ratio of the precursor hydrogel are similar,[18- 21] so questions arise as to how the 18C6 host-guest interactions dictate which zeolite crystallises.

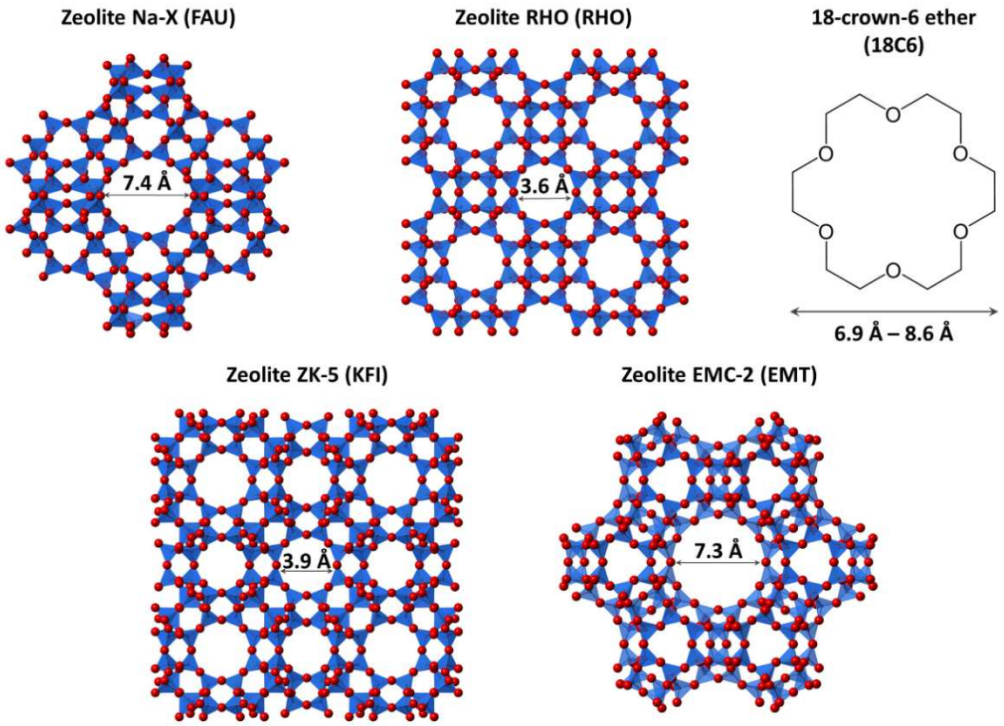

Figure 1. Polyhedral structures of the topologies of the four zeolite materials studied: zeolites Na-X, RHO, ZK-5, and EMC-2. Both zeolites RHO and ZK-5 are viewed down the *a* axis, Na-X along the (1.2, 1.2, 0) plane and EMC-2 down the *c* axis. These structures clearly show the channel geometries with labelled sizes of the pores which are occupied by 18-crown-6 ether.[21, 29-31] The chemical structure of 18-crown-6 ether (18C6) is also shown, as well as the approximate molecule size.[28]

Through a combination of thermogravimetry, mass spectrometry and differential thermal analysis, we demonstrate that all four zeolites show experimental differences in their host-guest interactions with 18C6. In addition, we have estimated the kinetics of 18C6 decomposition via the methods by Ozawa, Flynn and Wall,[32, 33] which is an approach that has not been used previously on zeolites.

methodology presented herein can be applied to understand the synthesis of current zeolites used in the petrochemical industry, such as those of the MFI-type. For example, both silicalite-1 and ZSM-5 can be prepared with a variety of organic templates,[34-36] which will all express different host-guest interactions which can be studied experimentally via the thermogravimetric and kinetic approaches used herein.

Experimental

Materials

The materials used in the synthesis of all four zeolites were colloidal silica (LUDOX® HS-40, 40 wt% SiO_2 suspension in water) as a silica source, distilled water as solvent and 18-crown-6 ether ($C_{12}H_{24}O_6$, 18C6) as organic additive. Amongst the syntheses, other materials used include sodium hydroxide (NaOH), potassium hydroxide (KOH), strontium nitrate ($Sr(NO_3)_2$) and aqueous caesium hydroxide (CsOH, 50wt% solution in water), as sources of cations and base. The source of alumina was either sodium aluminate ($NaAlO_2$) or aluminium hydroxide ($Al(OH)_3$). All materials were purchased from Sigma-Aldrich aside from the aluminium hydroxide, which was from ACROS.

Synthesis

The zeolites were prepared using previously reported methods: RHO,[20, 26] ZK-5[18] and EMC-2.[22, 23] Zeolite Na-X containing 18C6 was synthesised by following the same method for zeolite EMC-2, but with an increased concentration of sodium hydroxide in the hydrogel. This was to favour assembly of the FAU framework over the EMT framework of zeolite EMC-2, as we have described previously.[23] Table 1 summarises the hydrogel molar batch compositions used in the synthesis of the zeolites.

Table 1. Molar batch compositions of the hydrogels used to prepare each zeolite.

	Na_2O	K_2O	SrO	Cs_2O	Al_2O_3	SiO_2	18C6	H_2O
RHO	1.8			0.3	1.0	10	0.50	100
ZK-5		2.7	0.1		1.0	10	1.00	220
EMC-2	2.0				1.0	9.7	0.47	87
Na-X	3.0				1.0	9.6	0.47	91

For zeolites RHO, EMC-2 and Na-X the synthesis procedure was much the same. First, the relevant alkali metal hydroxides and 18C6 were dissolved in distilled water. The sodium aluminate was added to this solution and stirred until the solution became clear. Slowly the colloidal silica was poured into the solution, allowing gelation. The produced hydrogel was then stirred under ambient conditions for 4 hours (for Na-X) or 24 hours (RHO and EMC-2), before being transferred to a sealed vessel for hydrothermal treatment. For zeolites RHO and EMC-2 the vessel was a Teflon cup inside a stainless-steel autoclave, which was heated to 110°C for 8 and 12 days respectively. As for zeolite Na-X the hydrothermal vessel was a Naglene Teflon FEP bottle, which was heated to 100°C for 8 days. The crystallised material was then separated from the mother liquor via vacuum filtration and washed until the filtrate was of neutral pH. The material was also washed to ensure that no residue 18C6 was left on the crystal external surface. The powder was subsequently dried in a 100°C oven overnight and ground.

room temperature, with any water lost due to evaporation added to the solution. In a separate vessel, the strontium nitrate and 18C6 were dissolved in the remaining portion of distilled water. The colloidal silica was then slowly added to this solution. Once the silica solution was homogeneous, the alumina solution was quickly added to it. The resulting hydrogel was stirred for 30 minutes, before being transferred to a Teflon cup in a sealed stainless-steel autoclave and heated to 150°C for 5 days. The crystallised material was then filtered, washed, dried and ground following the same method as the other zeolites.

Metal Cation-Crown Complex Synthesis

Isolated complexes of the individual metal cations coordinated to the central cavity of the 18C6 molecule were synthesised. The molar ratio of metal salt to 18C6 was 2:1, to ensure that the metal cation would complex to the crown. The metal salts used were sodium hydroxide, potassium hydroxide and caesium hydroxide. Both the 18C6 and metal salt were dissolved in the minimum volume of distilled water and left to evaporate to propagate crystallisation. A strontium cation 18C6 complex was neglected, as due to trace quantities of the cation in the zeolite ZK-5 hydrogel it was deemed unlikely to form a significant concentration of a 18C6 complex.

Characterisation

Powder X-ray diffraction (PXRD) data were obtained with a Bruker D8-Advance X-ray powder diffractometer, using a Cu Kα radiation source of wavelength 1.5418 Å. The synthesised zeolite samples were indexed and identified using the simulated diffraction patterns collated by Treacy and Higgins.[37]

Thermogravimetric (TG) analysis and differential thermal analysis (DTA) were performed using a Setaram Setsys Evolution TGA 16/18. The evolving gas was analysed by mass spectrometry (MS) using a Pfeiffer Vacuum Omnistar GSD 320, equipped with a quadrupole mass analyser and a SEM detector. Samples were loaded into open alumina crucibles, 170 µL for the TG analysis and 100 µL for the DTA analysis. Samples were heated in an air atmosphere (flow rate of 20 $mlmin^{-1}$), from 30°C to 600°C at a ramp rate of 5 $Kmin^{-1}$. For analysis of the 18C6 mass content and apparent activation energy of zeolites EMC-2 and Na-X different ramping regimes were used to separate the 18C6 decomposition event from the water desorption. This was done by having an intermediate stage during ramping where the temperature was held constant to permit full water desorption before decomposition. This was 20 minutes at 180°C for zeolite EMC-2 and 60 minutes at 130°C for zeolite Na-X. A TG measurement was made on an empty crucible at a ramp of 5 $Kmin^{-1}$, however the instrument fluctuations on the mass were negligible in contrast to the mass changes observed throughout the 18C6 decomposition. Therefore, the instrument effects on the mass were not included in the subsequent calculations.

Mass spectrometry was first performed by scanning the m/z range from 0-200, to observe the array of fragments being produced during the decomposition. From this, the analysis was repeated but by tracking the m/z ions of 18, 32 and 44, which correspond to H_2O, O_2 and CO_2 respectively. Ions m/z 18 and 44 were used to track the decomposition of 18C6, whereas m/z 32 was used to observe the uptake of O_2 from the air flow.

the original work by Ozawa[32] concerns polymers, the method has not been restricted to one particular type of reaction. It is deemed that the method can be applied if the mass loss observed appears in one or separate steps. Presently, there are no recorded techniques to approximate the activation energy of organic additive decomposition in zeolites.

The onset of 18C6 decomposition was first determined by calculating the midpoint of the plateau between the water desorption and the decomposition. The offset was assumed to be the final point at 600°C, as at this temperature the decomposition must be complete. Taking the values between this range, the mass from the TG was converted into the variable 'Alpha' which represented the reaction coordinate. Before decomposition this value is 0.0 and once complete it is 1.0. This was done for each of the three ramp rates. At 0.1 intervals of 'Alpha' the inverse of the temperature at that Alpha value was plotted against the logarithm of the ramp rate. For each 'Alpha' value, this produced a straight line, the gradient of which was used to calculate the apparent activation energy, as following the ISO 11358-3:2014 standard procedure.

For zeolites RHO and ZK-5 the apparent activation energy reported was the average of the values at the Alpha intervals of 0.1, 0.2 and 0.3. As both zeolite Na-X and EMC-2 showed two phenomena in the decomposition, we attempted to calculate the activation energy of each event. Once the dTG/dt curves were separated into separate bands, Alpha intervals were chosen which closely represent the corresponding band – as opposed to the region where the bands overlap. For zeolite Na-X these were Alpha intervals of 0.1, 0.15 and 0.2 for band 1, and 0.8, 0.85 and 0.9 for band 2. For zeolite EMC-2 this was 0.1, 0.15 and 0.2 for band 1, and 0.7, 0.75 and 0.8 for band 2. The error in the apparent activation energy for each zeolite was taken as the standard deviation of the three values used to calculate the average.

Results and Discussion

First, we considered how the metal cations present in each zeolite could potentially coordinate to the cavity of the occluded 18C6 and influence the thermodynamics of decomposition. The cations to be considered are as follows: Na^+ for zeolites Na-X and EMC-2, Na^+ and Cs^+ for zeolite RHO, and K^+ for zeolite ZK-5. Initial thermogravimetric studies showed that the coordination of a metal cation to 18C6 has trivial influence on the decomposition temperature, as shown in table 2. The determined decomposition temperatures were observed to be within a ±19°C range from the vacant 18C6 molecule. Therefore, it was deemed that any coordinated cations to the occluded 18C6 would have a negligible influence on the decomposition process within the zeolites. The thermogravimetric and mass spectrometry curves of the vacant 18C6 and each of the metal cation complexes are included in the Supporting Information (SI).

Table 2. Decomposition temperatures of 18C6 and the three alkali metal cation complexes. Temperatures taken as the peak in the derivative of the thermogravimetric curve (dTG/dt) at a ramp rate of 5 $Kmin^{-1}$. Standard deviations were calculated from repeated scans.

	18C6	**(Na^+)18C6**	**(K^+)18C6**	**(Cs^+)18C6**
Decomposition Temperature /°C	203 (0.6)	193 (2.1)	223 (6.4)	206 (7.1)

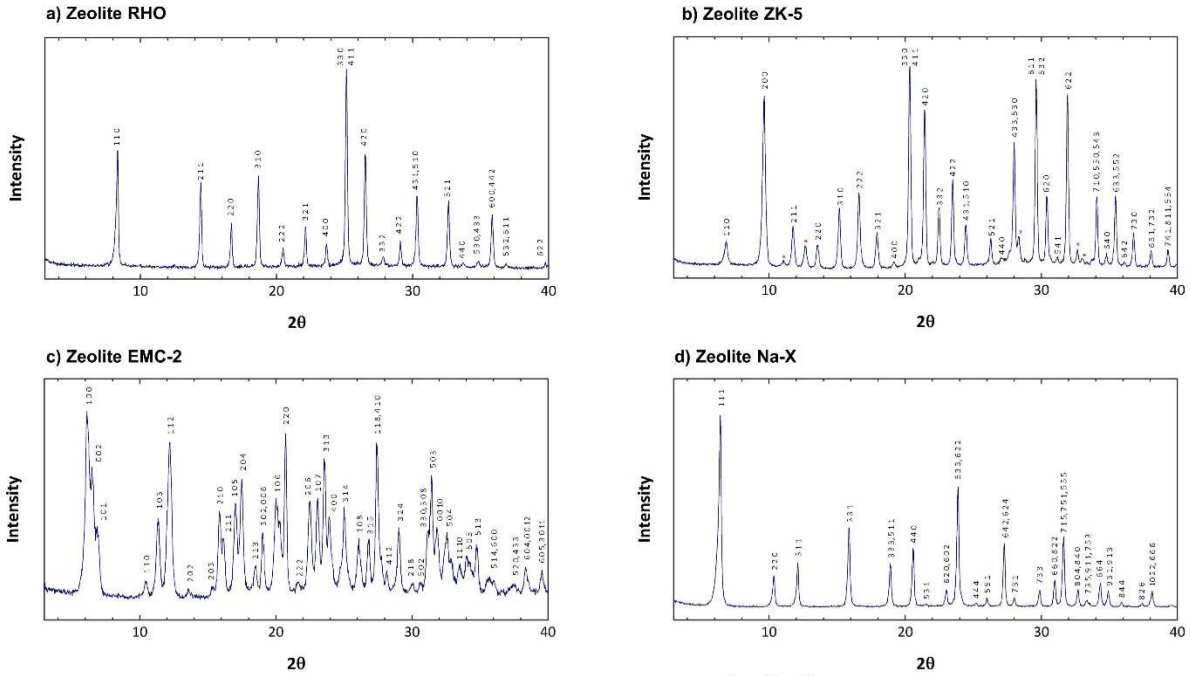

Figure 2. Powder X-ray diffraction (PXRD) patterns for the synthesised zeolites a) RHO, b) ZK-5, c) EMC-2 and d) Na-X. Bragg peaks are indexed to the corresponding phase. Peaks indexed with a red star correspond to a zeolite W impurity phase.

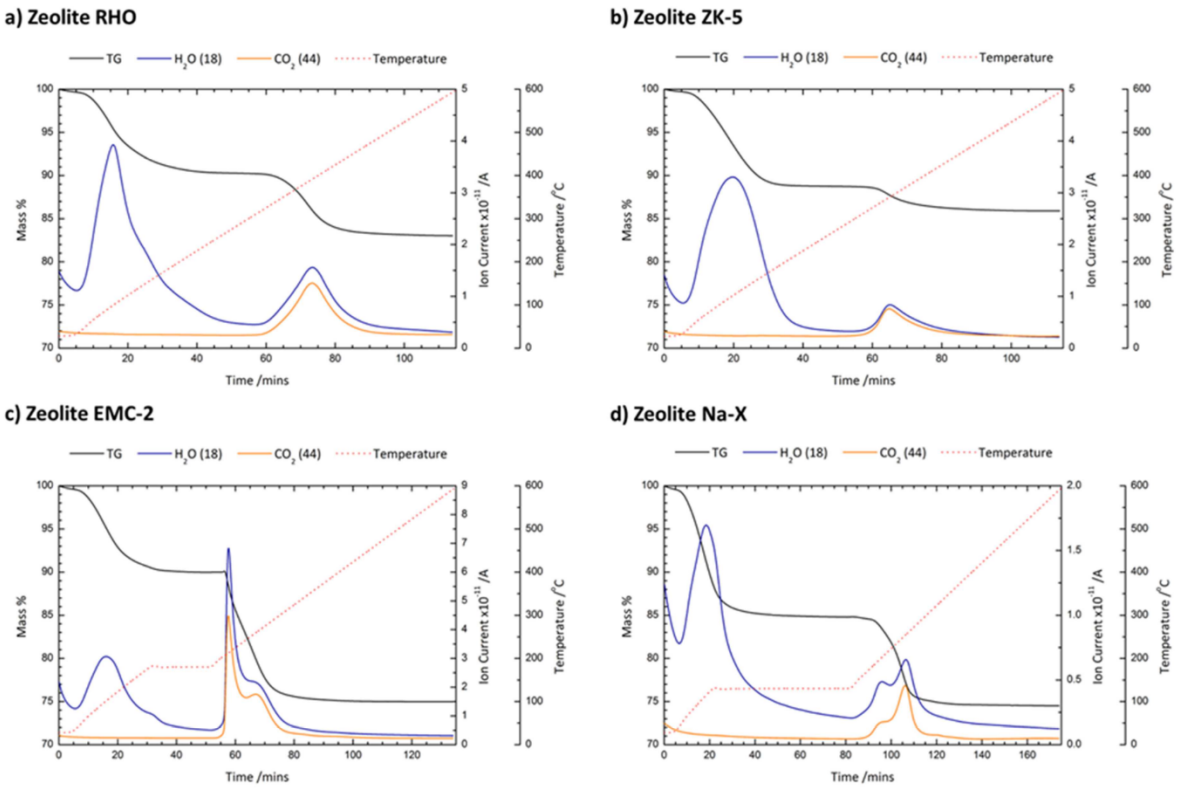

The four 18C6-containing zeolites were successfully crystallised, as shown by their indexed powder X-ray diffraction patterns in figure 2. The thermogravimetric (TG) curves of the four zeolites heated in air, at a ramp rate of 5 $Kmin^{-1}$ are shown in figure 3. The figure also shows the mass spectrometry (MS) signals of water and CO_2 liberated during the ramping cycle. All four zeolites show the initial desorption of extra-framework water, followed by the decomposition of the 18C6 molecule. At a constant ramp rate, it is observed that for zeolite EMC-2 and Na-X these two events overlap. Therefore, for these two samples the ramping regime included an intermediate stage of static temperature, to ensure that all the water is desorbed prior to 18C6 decomposition as is shown in figure 3. Larger scale TG-MS curves are included in the SI.

The four zeolites show unique TG decomposition curves, as well as different decomposition temperatures. Table 3 contains the 18C6 decomposition temperature and mass% content for each of the zeolites. All four zeolites contain different mass% contents of 18C6, which is dependent on the synthesis yield and the degree to which 18C6 is integrated into the growing framework. Interestingly, although zeolite ZK-5 contained the highest molar proportion of 18C6 in the hydrogel (table 1) it has the lowest mass% content in the crystallised product. Concerning the 18C6 decomposition temperature, it is seen to increase upon occlusion within a zeolite host. Furthermore, there is an inverse correspondence between the decomposition temperature and the zeolite pore size, with the smallest-pore zeolite RHO showing the highest 18C6 decomposition temperature. This demonstrates that more thermal energy is required to permit 18C6 decomposition in the smaller pore zeolites. Previous TG analysis of FAU and EMT framework zeolites by Feijen et al.[39] suggested the 18C6 decomposition temperature is dictated by Si/Al ratio and independent of the host's structure. However, with the inclusion of the smaller pore zeolites RHO and ZK-5 herein the full picture is that the framework geometry dominates the 18C6 decomposition temperature. The Si/Al ratio of our zeolite samples are reported in the SI for reference.

Table 3. Summary of the results from the TG analysis, including decomposition temperature, mass% content of 18C6 and apparent activation energy of decomposition. The 18C6 mass% content was taken as the average calculated from three separate runs at different ramp rates (2, 5 and 10 $Kmin^{-1}$), with the reported error being the standard deviation.

	Pore diameter[30] /Å	Max. diameter of an occluded sphere[40] / Å	Decomposition temperature /°C	18C6 content mass%	Activation energy (E_a) per mole of 18C6 /$kJmol^{-1}$
18C6			203 (6.0)		44.5 (0.39)
RHO	3.6	10.37	387 (0.30)	7.32 (0.09)	139 (2.4)
ZK-5	3.9	10.61	347 (1.4)	2.94 (0.12)	145 (5.1)
EMC-2	7.3 7.5x6.5	11.49	219 (9.1) 262 (1.7)	15.2 (0.07)	136 (5.9) 119 (1.3)
Na-X	7.4	11.18	204 (2.8) 256 (0.70)	10.3 (0.11)	124 (4.7) 128 (7.5)

Both zeolites RHO (figure 3a) and ZK-5 (figure 3b) show a decomposition of 18C6 that occurs in a single event, as shown by a single peak in the TG and MS curves. In zeolite RHO the MS signals for water and CO_2 follow a symmetric bell-curve shape; however in zeolite ZK-5 they are asymmetric with a tail at higher temperatures. This illustrates that the rate of decomposition slows down as it proceeds in zeolite ZK-5. This asymmetric shape was confirmed in the differential dTG/dt curve, as

Zeolite EMC-2 (Figure 3c) and Na-X (Figure 3d) show double peaks in the MS signals for water and CO_2 throughout 18C6 decomposition. This demonstrates that the decomposition occurs via a coherent two-event process, unlike what is seen with zeolites RHO and ZK-5. The presence of a two-event decomposition is further confirmed by the double peak shape of the derivative dTG/dt curves (see SI). As both zeolite EMC-2 and Na-X are the larger pore zeolites of the four, it is expected that the weaker host-guest interactions permit the accessibility of a lower temperature decomposition pathway.

For zeolite EMC-2 we also observed an additional, unique feature which has not been reported previously. Figure 3c shows an inflection point in the TG curve, where the decomposition of 18C6 occurs suddenly and rapidly. Prior to this rapid decomposition there is a slight mass increase, which is observed with repeated scans and at different ramp rates. This mass increase can be seen with the inset in figure 4 but is also emphasised by the spike in the derivative dTG/dt curve in the SI. Observing the MS signal in figure 4 for the m/z 32 ion, corresponding to O_2, there is a decrease in the signal concurrent with the mass increase. This is due to the oxidation of the 18C6 in the zeolite pores, being an initial step before the decomposition process. Such an observation compliments the suggested mechanism by Feijen et al.[39] where an ether bond undergoes cleavage to produce an opposing vinyl and hydroxyl group. The subsequent hump in the m/z 32 signal likely corresponds to methanol produced during the oxidation/decomposition process. This production of methanol, as well as a decrease in the O_2 signal, has not been seen for the other three zeolites. This further substantiates that the decomposition mechanism is different in zeolite EMC-2.

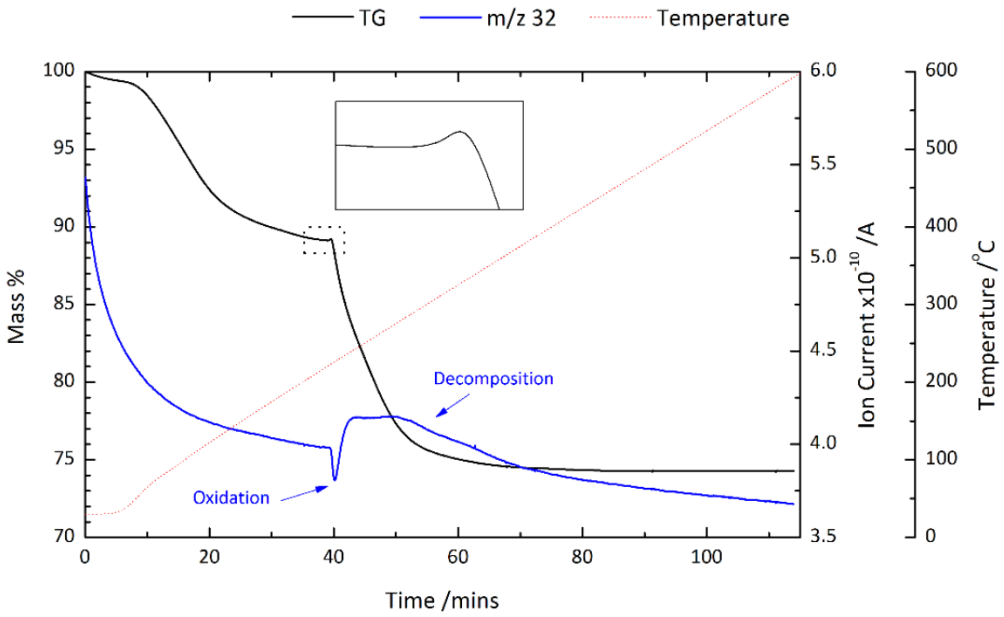

Figure 4. TG curve for zeolite EMC-2 heating at 5 Kmin^{-1}, alongside the MS signal of the m/z 32 ion for O_2. The inset includes a zoom in of the observed mass increase.

Although it is apparent that there is a relationship between the zeolite pore size and the

To address the thermodynamics of decomposition we obtained differential thermal analysis (DTA) curves of the four zeolites and the isolated 18C6, as shown in figure 5. The initial endothermic peak below 50°C seen for 18C6 corresponds to the phase change from solid to liquid. As for the exothermic peaks, the positions corroborate the decomposition temperatures that we have reported in table 3. In addition to this, the shapes of the curves are similar to their respective MS signals, with zeolite EMC-2 and Na-X showing a two-event decomposition whereas zeolite RHO and ZK-5 show single peaks. The double hump exotherms for zeolite EMC-2 and Na-X have also been reported by Feijen et al.[39] and Chatelain et al.[19] The fact that we observe exotherms for zeolite RHO and ZK-5 at the same position as the mass loss in the TG indicates that there is no initial 18C6 decomposition prior to liberation from the framework. This supports the inverse relationship between pore size and decomposition temperature.

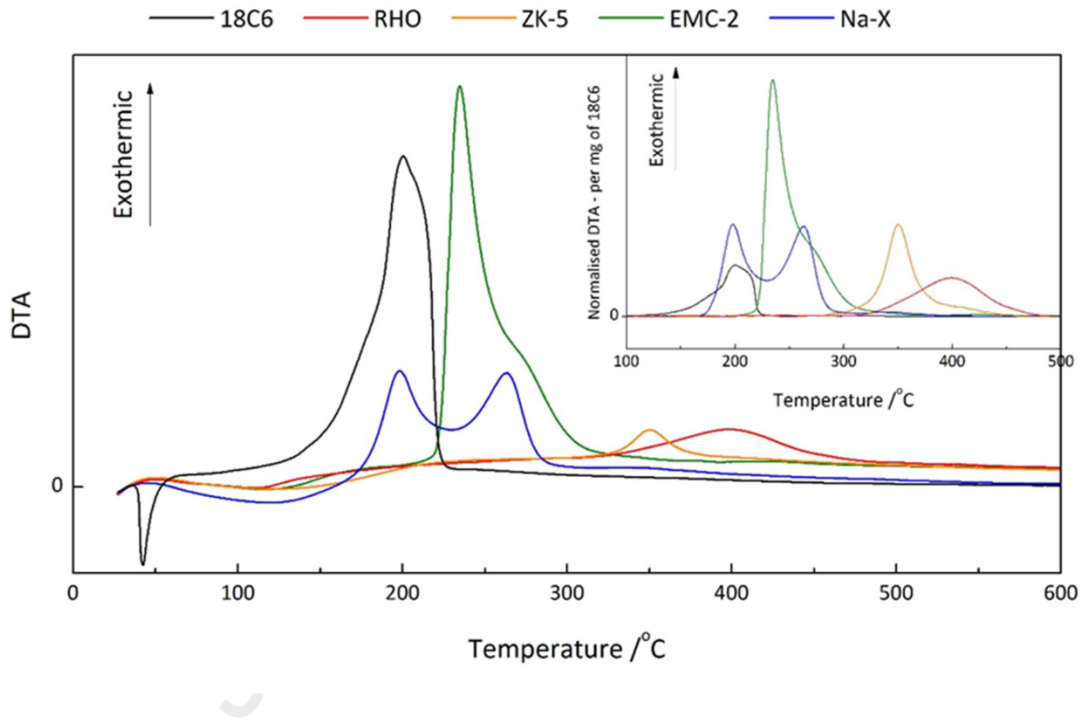

Figure 5. Differential thermal analysis (DTA) curves for the four zeolites and 18C6. The inset shows the same curves with the baseline removed manually using a polynomial function and normalizing the data to show the heatflow per mg of 18C6 in the sample. The area of each curve is an indicator of the energy released upon decomposition.

The inset in figure 5 illustrates that per mg of 18C6 the exotherm areas are substantially different, indicating differences in the enthalpy change of decomposition. The exotherm area increases in the order: RHO < ZK-5 < Na-X < EMC-2, which is consistent with the order of ascending framework cage volume and pore size. It can be assumed that the state of the decomposition products for each zeolite are comparable, as the MS signals of water and CO_2 in figure 3 have comparable areas and hence the water to CO_2 ratio is similar. Although the data suggests the decomposition pathway is different between the zeolites, Hess' Law dictates that the enthalpy change is irrespective of the pathway taken. Therefore, the initial environment of the occluded 18C6 molecule must be different in each framework, being dictated by the strength of the host-guest confinement interactions. In the

Concerning kinetics, we estimated the activation energy of 18C6 decomposition in each zeolite by recording the TG curve at different ramp rates. This was carried out using the technique reported by Ozawa, Flynn and Wall[32, 33] and explained in the Experimental section. These values are not true values for the activation energy, but rather a product of all the potential effects that can influence the kinetics of decomposition. Regardless, these values can still be used as an indicator of how the decomposition kinetics differ between the zeolites. The calculated apparent activation energies are shown in table 3. The apparent activation of decomposition is significantly greater when the 18C6 is occluded in a framework, as opposed to being isolated. This is anticipated, due to reduced access to oxygen which needs to diffuse through the zeolite channels. However, amongst the four zeolites there appears to be no significant difference in the energy. This indicates that even if the zeolite has smaller pores, with potentially limited oxygen transport, it does not have a significant influence on the kinetics of decomposition. Consequently, there is no correlation to the geometry of the host zeolite framework. This also appears to be the case if the decomposition pathway differs, as we have seen in zeolite EMC-2.

Conclusion

In summary, there is a clear distinction in the decomposition of the 18C6 molecule in the different zeolite frameworks. By using thermogravimetry and differential thermal analysis clear, experimental differences in the host-guest interactions between organic additives and zeolites hosts can be observed. Within the smaller pore/cage volume zeolites there are stronger host-guest confinement interactions which manifest as increased decomposition temperatures and lower decomposition enthalpy changes. There is also evidence to suggest that in the larger pore zeolites the 18C6 decomposition occurs via an alternative lower energy pathway.

This work is a crucial step in elucidating the discrepancies in host-guest interactions between organic additives and zeolite frameworks. Such experimental observations can therefore be used to support computer simulations when predicting favourable non-bonding interactions that are integral to framework assembly during crystallisation. Understanding the nature of these interactions is vital if we hope to take advantage of such interactions to prepare tailor-made zeolites. We propose that our methodology can be applied to other zeolites to explore differences in how organic additives interact with zeolite frameworks.

Data Availability

All data created during this research are openly available from the University of Bath data archive at https://doi.org/10.15125/BATH-00427.

Conflicts of Interest

There are no conflicts of issue to declare

Acknowledgements

A.S. thanks the Royal Society for funding. P.B.P. and A.N. thank the EPSRC for funding (grant number

Author Contributions

The manuscript was written by A.N. and proof read by all the co-authors. Sample preparation and analyses were per-formed by A.N. R.C. helped with the TG and DTA setup, in addition to the means of analysing and interpreting the data. Both A.S. and P.R.R. aided in the data interpretation.

References

1 P. A. Jacobs, E. M. Flanigen, J. C. Jansen and H. van Bekkum, Introduction to Zeolite Science and Practice, Elsevier Science, Amsterdam, 2010.

2 M. Zaarour, B. Dong, I. Naydenova, R. Retoux and S. Mintova, *Microporous and Mesoporous Materials*, 2014, **189**, 11-21.

3 M. E. Davis, *Nature*, 2002, **417**, 813-821.

4 V. Van Speybroeck, K. Hemelsoet, L. Joos, M. Waroquier, R. G. Bell and C. R. A. Catlow, *Chemical Society Reviews*, 2015, **44**, 7044-7111.

5 A. Sartbaeva, S. A. Wells, M. Treacy and M. Thorpe, *Nature Materials*, 2006, **5**, 962.

6 Y. Li, X. Li, J. Liu, F. Duan and J. Yu, *Nature Communications*, 2015, **6**, 8328.

7 L.-C. Lin, A. H. Berger, R. L. Martin, J. Kim, J. A. Swisher, K. Jariwala, C. H. Rycroft, A. S. Bhown, M. W. Deem and M. Haranczyk, *Nature Materials*, 2012, **11**, 633.

8 S. Curtarolo, G. L. Hart, M. B. Nardelli, N. Mingo, S. Sanvito and O. Levy, *Nature Materials*, 2013, **12**, 191.

9 P. Guo, J. Shin, A. G. Greenaway, J. G. Min, J. Su, H. J. Choi, L. Liu, P. A. Cox, S. B. Hong and P. A. Wright, *Nature*, 2015, **524**, 74.

10 *Science*, 2011, **334**, 1629-1635.

11 R. Barrer and P. Denny, *Journal of the Chemical Society (Resumed)*, 1961, 971-982.

12 R. L. Wadlinger, G. T. Kerr and E. J. Rosinski, US3308069A, 1967.

13 C. S. Cundy and P. A. Cox, *Microporous and Mesoporous Materials*, 2005, **82**, 1-78.

14 M. E. Davis and R. F. Lobo, *Chemistry of Materials*, 1992, **4**, 756-768.

15 D. W. Lewis, C. M. Freeman and C. R. A. Catlow, *Journal of Physical Chemistry*, 1995, **99**, 11194-11202.

16 R. F. Lobo, S. I. Zones and M. E. Davis, *Inclusion Chemistry with Zeolites: Nanoscale Materials by Design*, 1995, 47-78.

17 D. W. Lewis, D. J. Willock, C. R. A. Catlow, J. M. Thomas and G. J. Hutchings, *Nature*, 1996, **382**, 604-606.

18 T. Chatelain, J. Patarin, R. Farre, O. Petigny and P. Schulz, *Zeolites*, 1996, **17**, 328-333.

19 T. Chatelain, J. Patarin, M. Soulard, J. L. Guth and P. Schulz, *Zeolites*, 1995, **15**, 90-96.

20 T. Chatelain, J. Patarin, E. Fousson, M. Soulard, J. L. Guth and P. Schulz, *Microporous Materials*, 1995, **4**, 231-238.

21 T. Chatelain, J. Patarin, E. Brendlé, F. Dougnier, J. L. Guth and P. Schulz, *Studies in Surface Science and Catalysis*, 1997, **105**, 173-180

22 Structure Commission of the International Zeolite Association, *Verified Syntheses of Zeolitic Materials*, Elsevier Science, Amsterdam, Second Revised Edition edn., 2001.

23 A. Nearchou, P. Raithby and A. Sartbaeva, *Microporous and Mesoporous Materials*, 2018, **255**, 261-270.

24 A. Nearchou, M-L. U. Cornelius, Z. L. Jones, I. E. Collings, S. A. Wells, P. R. Raithby and A. Sartbaeva, *Royal Society open science*, 2019, **6**(7), 182158

25 S. F. Mousavi, M. Jafari, M. Kazemimoghadam and T. Mohammadi, *Ceramics International*, 2013, **39**, 7149-7158.

26 A. Nearchou and A. Sartbaeva, *Crystengcomm*, 2015, **17**, 2496-2503.

30 C. Baerlocher, L. B. McCusker and D. H. Olson, *Atlas of Zeolite Framework Types*, Elsevier, Amsterdam, 6th edn., 2007.
31 C. Baerlocher, L. B. McCusker and R. Chiappetta, *Microporous Materials*, 1994, **2**, 269-280.
32 T. Ozawa, *Bulletin of the Chemical Society of Japan*, 1965, **38**, 1881-1886.
33 J. H. Flynn and L. A. Wall, *Journal of Polymer Science Part C: Polymer Letters*, 1966, **4**, 323-328.
34 E. M. Flanigen, J. Bennett, R. Grose, J. Cohen, R. Patton, R. Kirchner and J. Smith, *Nature*, 1978, **271**, 512-516.
35 W. Xu, J. Dong, J. Li, J. Li and F. Wu, *Journal of the Chemical Society, Chemical Communications*, 1990, 755-756.
36 S. Sang, F. Chang, Z. Liu, C. He, Y. He and L. Xu, *Catalysis Today*, 2004, **93**, 729-734.
37 M. M. J. Treacy and J. B. Higgins, *Collection of Stimulated XRD Powder Patterns For Zeolites*, Elsevier, Amsterdam, 4th edn., 2001.
38 European Committee for Standardization. Plastics – Thermogravimetry (TG) of polymers – Part 1: General principles (ISO 11358-1:2014), (2014).
39 E. J. Feijen, J. A. Martens and P. A. Jacobs, *Journal of the Chemical Society, Faraday Transactions*, 1996, **92**, 3281-3285.
40 M. Foster, I. Rivin, M. Treacy and O. D. Friedrichs, *Microporous and Mesoporous Materials*, 2006, **90**, 32-38.
41 S. Liu, P. Zhang, X. Meng, D. Liang, N. Xiao and F.-S. Xiao, *Microporous and Mesoporous Materials*, 2010, **132**, 352-356.

Highlights:

- thermogravimetric and differential thermal analysis techniques were used to study the crown ether decomposition in four zeolites
- there is a clear distinction in the decomposition of the 18C6 molecule in the different frameworks
- measurable differences are seen in the host-guest interactions between organic additives and zeolite hosts
- stronger host-guest confinement interactions are seen in zeolites with smaller pores
- our methodology can be applied to other zeolites to study the host-guest interactions

Declaration of interests

☒ The authors declare that they have no known competing financial interests or personal relationships that could have appeared to influence the work reported in this paper.

☐The authors declare the following financial interests/personal relationships which may be considered as potential competing interests: